Reconstruction Algorithms for Positron Emission Tomography and Single Photon Emission Computed Tomography and their Numerical Implementation

A.S. Fokas, A. Iserles and V. Marinakis
Department of Applied Mathematics and
Theoretical Physics, University of Cambridge
Cambridge, CB3 0WA, United Kingdom

Abstract

The modern imaging techniques of Positron Emission Tomography and of Single Photon Emission Computed Tomography are not only two of the most important tools for studying the functional characteristics of the brain, but they now also play a vital role in several areas of clinical medicine, including neurology, oncology and cardiology. The basic mathematical problems associated with these techniques are the construction of the inverse of the Radon transform and of the inverse of the so called attenuated Radon transform respectively. We first show that, by employing mathematical techniques developed in the theory of nonlinear integrable equations, it is possible to obtain analytic formulas for these two inverse transforms. We then present algorithms for the numerical implementation of these analytic formulas, based on approximating the given data in terms of cubic splines. Several numerical tests are presented which suggest that our algorithms are capable of producing accurate reconstruction for realistic phantoms such as the well known Shepp–Logan phantom.

1 Introduction

Positron emission tomography (PET) and single photon emission computed tomography (SPECT) are two modern imaging techniques with a wide range of medical applications. Although these techniques were originally developed for the study of the *functional* characteristics of the brain, they are now used in many diverse areas of clinical medicine. For example a recent editorial in the New England Journal of Medicine [1] emphasized the importance of PET in oncologic imaging. Other medical applications of PET and SPECT are presented in [2]–[22].

The first step in PET is to inject the patient with a dose of a suitable radiopharmaceutical. For example in brain imaging a typical such radiopharmaceutical is flurodeoxyglucose (FDG), which is a normal molecule of glucose attached artificially to an atom of radioactive fluorine. The cells in the brain which are more active have a higher metabolism, need

more energy, thus will absorb more FDG. The fluorine atom in the FDG molecule suffers a radioactive decay, emitting a positron. When a positron collides with an electron it liberates energy in the form of *two* beams of gamma rays travelling in *opposite* direction, which are picked by the PET scanner. SPECT is similar to PET but the radiopharmaceuticals decay to emit a *single* photon.

In both PET and SPECT the radiating sources are inside the body, and the aim is to determine the distribution $g(x_1, x_2)$ of the relevant radiopharmaceutical from measurements made outside the body of the emitted radiation. If $f(x_1, x_2)$ is the x–ray attenuation coefficient of the body, then it is straightforward to show [23] that the intensity I outside the body measured by a detector which picks up only radiation along the straight line L is given by

$$I = \int_L \mathrm{e}^{-\int_{L(x)} f \mathrm{d}s} g \mathrm{d}\tau \tag{1.1}$$

where τ is a parameter along L, and $L(x)$ denotes the section of L between the point (x_1, x_2) and the detector. The attenuation coefficient $f(x_1, x_2)$ is precisely the function measured by the usual computed tomography. Thus the basic mathematical problem in SPECT is to determine the function $g(x_1, x_2)$ from the knowledge of the "transmission" function $f(x_1, x_2)$ (determined via computed tomography) and the "emission" function I (known from the measurements).

In PET the situation is simpler. Indeed, since the sources eject particles *pairwise* in *opposite* directions and the radiation in opposite directions is measured *simultaneously*, equation (1.1) is replaced by

$$I = \int_L \mathrm{e}^{-\int_{L_+(x)} f \mathrm{d}s - \int_{L_-(x)} f \mathrm{d}s} g \mathrm{d}\tau, \tag{1.2}$$

where L_+, L_- are the two half–lines of L with endpoint x. Since $L_+ + L_- = L$, equation (1.2) becomes

$$I = \mathrm{e}^{-\int_L f \mathrm{d}\tau} \int_L g \mathrm{d}\tau.$$

We recall that the line integral of the function $f(x_1, x_2)$ along L is precisely what is known from the measurements in the usual computed tomography. Thus since both I and the integral of $f(x_1, x_2)$ are known (from the measurements of SPECT and of computed tomography respectively), the basic mathematical problem of PET is to determine $g(x_1, x_2)$ from the knowledge of its line integrals. This mathematical problem is identical with the basic mathematical problem of computed tomography.

Notation

(i) A point of a line L making an angle θ with the x_1–axis is specified by the three real numbers (τ, ρ, θ), where τ is a parameter along L, $-\infty < \tau < \infty$, ρ is the distance from the origin to the line, $-\infty < \rho < \infty$, and $0 \leq \theta \leq 2\pi$.
(ii) The above parameterization implies that, for a fixed θ, the Cartesian coordinates (x_1, x_2) can be expressed in terms of the *local coordinates* (τ, ρ) by the equations (see Section 2)

$$x_1 = \tau \cos\theta - \rho \sin\theta, \quad x_2 = \tau \sin\theta + \rho \cos\theta. \tag{1.3}$$

A function $f(x_1, x_2)$ rewritten in local coordinates will be denoted by $F(\tau, \rho, \theta)$,

$$F(\tau, \rho, \theta) = f(\tau \cos\theta - \rho \sin\theta, \tau \sin\theta + \rho \cos\theta).$$

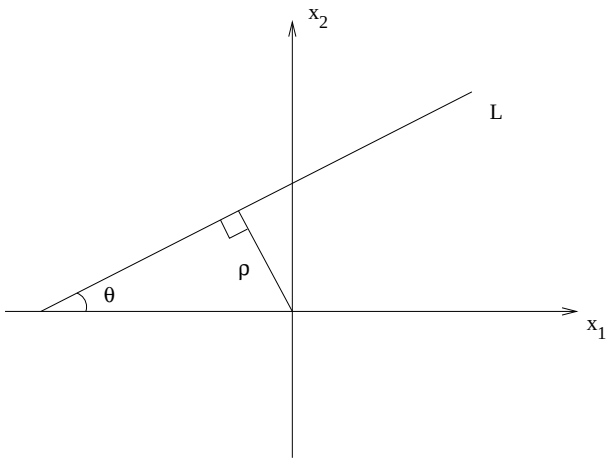

Figure 1: Local coordinates for the mathematical formulation of PET and SPECT.

Thus $F(\tau,\rho,\theta)$ and $G(\tau,\rho,\theta)$ will denote the x–ray attenuation coefficient $f(x_1,x_2)$ and the distribution of the radiopharmaceutical $g(x_1,x_2)$, rewritten in local coordinates.
(iii) The line integral of a function f is called its *Radon transform* and will be denoted by $\hat{f}$. In order to compute $\hat{f}$, we first write f in local coordinates and then integrate with respect to τ,

$$\hat{f}(\rho,\theta)=\int_{-\infty}^{\infty}F(\tau,\rho,\theta)\mathrm{d}\tau. \tag{1.4}$$

The line integral of the function g with respect to the weight f appearing in equation (1.1) is called the *attenuated Radon transform* of g (with the attenuation specified by f) and will be denoted by $\hat{g}_f$. In order to compute $\hat{g}_f$, we write both g and f in local coordinates and then evaluate the following integral

$$\hat{g}_f(\rho,\theta)=\int_{-\infty}^{\infty}\mathrm{e}^{-\int_\tau^\infty F(s,\rho,\theta)\mathrm{d}s}G(\tau,\rho,\theta)\mathrm{d}\tau. \tag{1.5}$$

Mathematical Methods

The basic mathematical problem of both computed tomography and PET is to reconstruct a function f from the knowledge of its Radon transform $\hat{f}$, i.e. to solve equation (1.4) for $f(x_1,x_2)$ in terms of $\hat{f}(\rho,\theta)$. The relevant formula is called the *inverse Radon transform* and is given by

$$f(x_1,x_2)=\frac{1}{4\mathrm{i}\pi^2}(\partial_{x_1}-\mathrm{i}\partial_{x_2})\int_0^{2\pi}\mathrm{e}^{\mathrm{i}\theta}\left(\fint_{-\infty}^{\infty}\frac{\hat{f}(\rho,\theta)\mathrm{d}\rho}{\rho-(x_2\cos\theta-x_1\sin\theta)}\right)\mathrm{d}\theta, \tag{1.6}$$

where $-\infty<x_j<\infty$, $j=1,2$ and $\fint$ denotes principal value integral.

A novel approach for deriving equation (1.6) was introduced in [24], and is based on the analysis of the equation

$$\left(\frac{1}{2}\left(\lambda+\frac{1}{\lambda}\right)\partial_{x_1}+\frac{1}{2\mathrm{i}}\left(\lambda-\frac{1}{\lambda}\right)\partial_{x_2}\right)\mu(x_1,x_2,\lambda)=f(x_1,x_2), \tag{1.7}$$

where λ is a complex parameter different than zero. The application of this approach to a slight generalization of equation (1.7) can be used to reconstruct a function g from the

knowledge of its attenuated Radon transform $\hat{g}_f$, i.e. this approach can be used to solve equation (1.5) for $g(x_1, x_2)$ in terms of $\hat{g}_f(\rho, \theta)$ and $f(x_1, x_2)$. The relevant formula, called the *inverse attenuated Radon transform*, was obtained by R. Novikov [25] by analysing, instead of equation (1.7), the equation

$$\left(\frac{1}{2}\left(\lambda + \frac{1}{\lambda}\right)\partial_{x_1} + \frac{1}{2\mathrm{i}}\left(\lambda - \frac{1}{\lambda}\right)\partial_{x_2} + f(x_1, x_2)\right)\mu(x_1, x_2, \lambda) = g(x_1, x_2). \tag{1.8}$$

Organization of the Paper

In Section 2 we first review the analysis of equation (1.7), and then show that if one uses the basic result obtained in this analysis, it is possible to construct immediately the inverse attenuated Radon transform. In Section 3 we present a new numerical reconstruction algorithm for both PET and SPECT. This algorithm is based on approximating the given data in terms of cubic splines. We recall that both the exact inverse Radon transform as well as the exact inverse attenuated Radon transform involve the Hilbert transform of the data functions. For example, the inverse Radon transform involves the function

$$h(\rho, \theta) = \fint_{-\infty}^{\infty} \frac{\hat{f}(\rho', \theta)}{\rho' - \rho} \mathrm{d}\rho'. \tag{1.9}$$

Existing numerical approaches use the convolution property of the Fourier transform to compute the Hilbert transform and employ appropriate filters to eliminate high frequencies. It appears that our approach has the advantage of simplifying considerably the mathematical formulas associated with these techniques. Furthermore, accurate reconstruction is achieved, for noiseless data, with the additional use of an averaging or of a median filter. Several numerical tests are presented in Section 4. One of these tests involves the Shepp–Logan phantom [26], see Figure 3(c).

Numerical algorithms based on the filtered back projection are discussed in [27]–[30], while algorithms based on iterative techniques can be found in [31]–[33].

2 Mathematical Methods

We first review the basic result of [24]. It will be shown later that using this result it is possible to derive both the inverse Radon as well as the inverse attenuated Radon transforms in a straightforward manner.

Proposition 2.1. Define the complex variable z by

$$z = \frac{1}{2\mathrm{i}}\left(\lambda - \frac{1}{\lambda}\right)x_1 - \frac{1}{2}\left(\lambda + \frac{1}{\lambda}\right)x_2, \tag{2.1}$$

where x_1, x_2 are the real Cartesian coordinates $-\infty < x_j < \infty$, $j = 1, 2$, and λ is a complex variable, $\lambda \neq 0$. Assume that the function $f(x_1, x_2)$ has sufficient decay as $|x_1| + |x_2| \to \infty$. Let $\mu(x_1, x_2, \lambda)$ satisfy the equation

$$\frac{1}{2\mathrm{i}}\left(\frac{1}{|\lambda|^2} - |\lambda|^2\right)\frac{\partial \mu(x_1, x_2, \lambda)}{\partial \bar{z}} = f(x_1, x_2), \quad |\lambda| \neq 1, \quad (x_1, x_2) \in \mathbb{R}^2, \tag{2.2}$$

as well as the boundary condition $\mu = \mathrm{O}(1/z)$ as $|x_1| + |x_2| \to \infty$. Let λ^+ and λ^- denote the limits of λ as it approaches the unit circle from inside and outside the unit disc respectively, i.e.

$$\lambda^{\pm} = \lim_{\varepsilon \to 0} (1 \mp \varepsilon) \mathrm{e}^{\mathrm{i}\theta}, \quad \varepsilon > 0, \quad 0 \le \theta \le 2\pi.$$

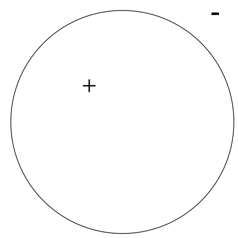

Figure 2: The unit circle.

Then

$$\mu(x_1, x_2, \lambda^{\pm}) = \mp P^{\mp} \hat{f}(\rho, \theta) - \int_{\tau}^{\infty} F(\tau', \rho, \theta) \mathrm{d}\tau', \tag{2.3}$$

where $\hat{f}$ denotes the Radon transform of f, F denotes f in the local coordinates (see the Notation in Section 1), $P^{\pm}$ denote the usual projection operators in the variable ρ, i.e.

$$(P^{\pm} g)(\rho) = \lim_{\substack{\varepsilon \to 0 \\ \varepsilon > 0}} \frac{1}{2\pi \mathrm{i}} \int_{-\infty}^{\infty} \frac{g(\rho') \mathrm{d}\rho'}{\rho' - (\rho \pm \mathrm{i}\varepsilon)} = \pm \frac{g(\rho)}{2} + \frac{1}{2\pi \mathrm{i}} \oint_{-\infty}^{\infty} \frac{g(\rho') \mathrm{d}\rho'}{\rho' - \rho}, \tag{2.4}$$

and $\oint$ denotes the principal value integral.

Proof. Before deriving this result, we first note that equation (2.1) is a direct consequence of equation (1.7). Indeed, equation (1.7) motivates the introduction of the variable z defined by equation (2.1). Taking the complex conjugate of equation (2.1) we find

$$\bar{z} = -\frac{1}{2\mathrm{i}} \left(\bar{\lambda} - \frac{1}{\bar{\lambda}} \right) x_1 - \frac{1}{2} \left(\bar{\lambda} + \frac{1}{\bar{\lambda}} \right) x_2. \tag{2.5}$$

Equations (2.1) and (2.5) define a change of variables from (x_1, x_2) to $(z, \bar{z})$. Using this change of variables to compute ∂_{x_1} and ∂_{x_2} in terms of ∂_z and $\partial_{\bar{z}}$, equation (1.7) becomes (2.2).

We now derive equation (2.3). The derivation is based on the following two steps, which have been used extensively in the field of nonlinear integrable PDEs, see for example [34].

(i) In the first step (sometimes called the direct problem), we consider equation (2.2) as an equation which defines μ in terms of f, and we construct an integral representation of μ in terms of f, for *all complex* values of λ. This representation is

$$\mu(x_1, x_2, \lambda) = \frac{1}{2\pi \mathrm{i}} \mathrm{sgn}\left(\frac{1}{|\lambda|^2} - |\lambda|^2 \right) \iint_{\mathbb{R}^2} \frac{f(x_1', x_2')}{z' - z} \mathrm{d}x_1' \mathrm{d}x_2', \quad |\lambda| \ne 1. \tag{2.6}$$

Indeed, suppose that the function $\mu(z_R, z_I)$ satisfies the equation

$$\frac{\partial \mu(z_R, z_I)}{\partial \bar{z}} = g(z_R, z_I), \quad z = z_R + \mathrm{i} z_I, \quad -\infty < z_R < \infty, \quad -\infty < z_I < \infty,$$

as well as the boundary condition $\mu = \mathrm{O}(1/z)$ as $z \to \infty$. Then Pompieu's formula (see for example [35]) implies

$$\mu = -\frac{1}{\pi} \iint\limits_{\mathbb{R}^2} \frac{g(z'_R, z'_I)}{z' - z} \mathrm{d}z'_R \mathrm{d}z'_I. \tag{2.7}$$

In our case

$$g = \frac{2\mathrm{i}f}{\frac{1}{|\lambda|^2} - |\lambda|^2}, \quad \mathrm{d}z_R \mathrm{d}z_I = \frac{1}{2\mathrm{i}} \left(\frac{1}{|\lambda|^2} - |\lambda|^2 \right) \mathrm{d}x_1 \mathrm{d}x_2,$$

thus equation (2.7) becomes (2.6).

(ii) In the second step (sometimes called the inverse problem), we analyze the analyticity properties of μ with respect to λ, and we find an *alternative* representation for μ. This representation involves certain integrals of f called spectral functions. For our problem, this representation is equation (2.3). Indeed, since μ is an analytic function of λ for $|\lambda| \neq 1$ and since $\mu = \mathrm{O}(1/\lambda)$ as $\lambda \to \infty$, we can reconstruct the function μ if we know its "jump" across the unit circle:

$$\mu(x_1, x_2, \lambda) = \frac{1}{2\pi} \int_0^{2\pi} \frac{J(x_1, x_2, \theta') \mathrm{e}^{\mathrm{i}\theta'}}{\mathrm{e}^{\mathrm{i}\theta'} - \lambda} \mathrm{d}\theta', \tag{2.8}$$

where

$$J(x_1, x_2, \theta) = \mu(x_1, x_2, \lambda^+) - \mu(x_1, x_2, \lambda^-).$$

Thus we need to compute the limits of μ as λ tends to $\lambda^\pm$. As $\varepsilon \to 0$,

$$\lambda^+ \mp \frac{1}{\lambda^+} \sim (1 - \varepsilon)\mathrm{e}^{\mathrm{i}\theta} \mp (1 + \varepsilon)\mathrm{e}^{-\mathrm{i}\theta}.$$

Substituting this expression in the definition of z (equation (2.1)) and simplifying, we find

$$z' - z \sim (x'_1 - x_1)\sin\theta - (x'_2 - x_2)\cos\theta + \mathrm{i}\varepsilon((x'_1 - x_1)\cos\theta + (x'_2 - x_2)\sin\theta). \tag{2.9}$$

The right–hand side of this equation can be rewritten in terms of the local coordinates ρ, ρ', τ, τ': Let $\mathbf{k}$ and $\mathbf{k}^\perp$ denote two unit vectors along the line L and perpendicular to this line, respectively. Then

$$\mathbf{x} = \tau\mathbf{k} + \rho\mathbf{k}^\perp,$$

or

$$(x_1, x_2) = \tau(\cos\theta, \sin\theta) + \rho(-\sin\theta, \cos\theta).$$

Hence x_1 and x_2 are given by equations (1.3). Inverting these equations we find

$$\tau = x_2 \sin\theta + x_1 \cos\theta, \quad \rho = x_2 \cos\theta - x_1 \sin\theta. \tag{2.10}$$

Thus equation (2.9) becomes

$$z' - z \sim -\rho' + \rho + \mathrm{i}\varepsilon(\tau' - \tau).$$

Substituting this expression in equation (2.6) and using the fact that the relevant sign equals 1, we find

$$\mu(x_1, x_2, \lambda^+) \sim -\frac{1}{2\pi\mathrm{i}} \iint\limits_{\mathbb{R}^2} \frac{f(x'_1, x'_2)\mathrm{d}x'_1\mathrm{d}x'_2}{\rho' - \rho - \mathrm{i}\varepsilon(\tau' - \tau)}, \quad \varepsilon \to 0, \quad \varepsilon > 0. \tag{2.11}$$

Using the change of variables $(x_1, x_2) \leftrightarrow (\tau, \rho)$ defined by equations (1.3) and (2.10), and noting that the relevant Jacobian is 1, i.e.

$$f(x_1', x_2')\mathrm{d}x_1'\mathrm{d}x_2' = F(\tau', \rho', \theta)\mathrm{d}\tau'\mathrm{d}\rho',$$

we find that the right–hand side of equation (2.11) equals

$$-\frac{1}{2\mathrm{i}\pi}\iint\limits_{\mathbb{R}^2} \frac{F\mathrm{d}\tau'\mathrm{d}\rho'}{\rho' - (\rho + \mathrm{i}\varepsilon(\tau' - \tau))}. \tag{2.12}$$

In order to simplify this expression we split the integral over $\mathrm{d}\tau'$ in the form

$$\int_{-\infty}^{\infty} \mathrm{d}\tau' = \int_{-\infty}^{\tau} \mathrm{d}\tau' + \int_{\tau}^{\infty} \mathrm{d}\tau',$$

and note that in the first integral $\tau' - \tau < 0$, while in the second integral $\tau' - \tau > 0$. Thus, using the second set of equations (2.4) the expression in (2.12) becomes

$$-\frac{1}{2\pi\mathrm{i}}\int_{-\infty}^{\infty}\left(\oint_{-\infty}^{\infty} F(\tau', \rho', \theta)\frac{\mathrm{d}\rho'}{\rho' - \rho}\right)\mathrm{d}\tau' - \frac{1}{2}\int_{\tau}^{\infty} F(\tau', \rho, \theta)\mathrm{d}\tau' + \frac{1}{2}\int_{-\infty}^{\tau} F(\tau', \rho, \theta)\mathrm{d}\tau'.$$

Finally, adding and subtracting the integral $\frac{1}{2}\int_{\tau}^{\infty}$ we find

$$\begin{aligned}\mu(x_1, x_2, \lambda^+) \;=\; & -\frac{1}{2\pi\mathrm{i}}\int_{-\infty}^{\infty}\left(\oint_{-\infty}^{\infty} F(\tau', \rho', \theta)\frac{\mathrm{d}\rho'}{\rho' - \rho}\right)\mathrm{d}\tau' \\ & + \frac{1}{2}\int_{-\infty}^{\infty} F(\tau', \rho, \theta)\mathrm{d}\tau' - \int_{\tau}^{\infty} F(\tau', \rho, \theta)\mathrm{d}\tau'.\end{aligned}$$

The first two terms in the right–hand side of this equation equal $-P^-\hat{f}$, hence we find $(2.3)^+$. The derivation of equation $(2.3)^-$ is similar. **QED**

Using equation (2.3) it is now straightforward to derive both the inverse Radon and the inverse attenuated Radon transforms. In this respect we note that the result of Proposition 2.1 can be rewritten in the form

$$\lim_{\lambda \to \lambda^{\pm}}\left\{\partial_{\bar{z}}^{-1}\left(\frac{f(x_1, x_2)}{\nu(\lambda)}\right)\right\} = \mp P^{\mp}\hat{f}(\rho, \theta) - \int_{\tau}^{\infty} F(\tau', \rho, \theta)\mathrm{d}\tau', \tag{2.13}$$

where

$$\nu(\lambda) = \frac{1}{2\mathrm{i}}\left(\frac{1}{|\lambda|^2} - |\lambda|^2\right). \tag{2.14}$$

The Inverse Radon Transform

Equations (2.3) yield

$$J(x_1, x_2, \theta) = -\frac{1}{\pi\mathrm{i}}\oint_{-\infty}^{\infty} \frac{\hat{f}(\rho', \theta)\mathrm{d}\rho'}{\rho' - (x_2\cos\theta - x_1\sin\theta)}. \tag{2.15}$$

Equation (2.8) implies

$$\mu(x_1, x_2, \lambda) = \left(-\frac{1}{2\pi}\int_0^{2\pi} J(x_1, x_2, \theta)\mathrm{e}^{\mathrm{i}\theta}\mathrm{d}\theta\right)\frac{1}{\lambda} + \mathrm{O}\left(\frac{1}{\lambda^2}\right).$$

Substituting this expression in equation (1.7) we find

$$f(x_1,x_2)=\frac{1}{2}(\partial_{x_1}-\mathrm{i}\partial_{x_2})\left(-\frac{1}{2\pi}\int_0^{2\pi}J(x_1,x_2,\theta)\mathrm{e}^{\mathrm{i}\theta}\mathrm{d}\theta\right). \tag{2.16}$$

Replacing in this equation J by the right–hand side of equation (2.15) we find equation (1.6).

The Attenuated Radon Transform

Equation (1.8) can be rewritten in the form

$$\frac{\partial\mu}{\partial\bar{z}}+\frac{f}{\nu}\mu=\frac{g}{\nu},$$

where ν is defined by equation (2.14). Hence

$$\frac{\partial}{\partial\bar{z}}\left(\mu\exp\left[\partial_{\bar{z}}^{-1}\left(\frac{f}{\nu}\right)\right]\right)=\frac{g}{\nu}\exp\left[\partial_{\bar{z}}^{-1}\left(\frac{f}{\nu}\right)\right],$$

or

$$\mu\exp\left[\partial_{\bar{z}}^{-1}\left(\frac{f}{\nu}\right)\right]=\partial_{\bar{z}}^{-1}\left(\frac{g}{\nu}\exp\left[\partial_{\bar{z}}^{-1}\left(\frac{f}{\nu}\right)\right]\right).$$

Replacing in this equation $\partial_{\bar{z}}^{-1}\left(\frac{f}{\nu}\right)$ by the right–hand side of equation (2.13) we find

$$\mu(x_1,x_2,\lambda^{\pm})\mathrm{e}^{\mp P^{\mp}\hat{f}(\rho,\theta)}\mathrm{e}^{-\int_\tau^\infty F(\tau',\rho,\theta)\mathrm{d}\tau'}=\partial_{\bar{z}}^{-1}\left(\frac{g(x_1,x_2)}{\nu(\lambda)}\mathrm{e}^{\mp P^{\mp}\hat{f}(\rho,\theta)}\mathrm{e}^{-\int_\tau^\infty F(\tau',\rho,\theta)\mathrm{d}\tau'}\right).$$

For the computation of the right–hand side of this equation we use again equation (2.13), where f is replaced by g times the two exponentials appearing in the above relation. Hence

$$\begin{aligned}&\mu(x_1,x_2,\lambda^{\pm})\mathrm{e}^{\mp P^{\mp}\hat{f}(\rho,\theta)}\mathrm{e}^{-\int_\tau^\infty F(\tau',\rho,\theta)\mathrm{d}\tau'}=\\&\quad\mp P^{\mp}\mathrm{e}^{\mp P^{\mp}\hat{f}(\rho,\theta)}\hat{g}_f(\rho,\theta)-\int_\tau^\infty G(\tau'\rho,\theta)\mathrm{e}^{\mp P^{\mp}\hat{f}(\rho,\theta)}\mathrm{e}^{-\int_{\tau'}^\infty F(s,\rho,\theta)\mathrm{d}s}\mathrm{d}\tau'.\end{aligned} \tag{2.17}$$

Note that the term $\exp[\mp P^{\mp}\hat{f}]$ is independent of τ', thus this term comes out of the integral $\int_\tau^\infty$, and furthermore the same term appears in the left–hand side of equation (2.17). Hence when computing the jump $\mu(x_1,x_2,\lambda^+)-\mu(x_1,x_2,\lambda^-)$, the second term in the right–hand side of equation (2.17) cancels and we find that the relevant jump in now given by

$$J(x_1,x_2,\theta)=-\mathrm{e}^{\int_\tau^\infty F(\tau',\rho,\theta)\mathrm{d}\tau'}\left(\mathrm{e}^{P^-\hat{f}(\rho,\theta)}P^-\mathrm{e}^{-P^-\hat{f}(\rho,\theta)}+\mathrm{e}^{-P^+\hat{f}(\rho,\theta)}P^+\mathrm{e}^{P^+\hat{f}(\rho,\theta)}\right)\hat{g}_f(\rho,\theta) \tag{2.18}$$

where τ and ρ are expressed in terms of x_1 and x_2 by equations (2.10).

Equation (2.8) is still valid, furthermore equation (2.16) is valid if f is replaced by g. Hence replacing in equation (2.16) f by g we find

$$g(x_1,x_2)=-\frac{1}{4\pi}(\partial_{x_1}-\mathrm{i}\partial_{x_2})\int_0^{2\pi}J(x_1,x_2,\theta)\mathrm{e}^{\mathrm{i}\theta}\mathrm{d}\theta, \tag{2.19}$$

where J is defined by equation (2.18). This formula is equivalent to Novikov's formula.

In summary, let $\hat{g}_f(\rho,\theta)$ be defined by equation (1.5), let $F(\tau,\rho,\theta)$ denote the function $f(x_1,x_2)$ written in local coordinates (see the Notation) and let $\hat{f}(\rho,\theta)$ denote the Radon transform of $f(x_1,x_2)$ (see equation (1.4)). Then $g(x_1,x_2)$ is given by equation (2.19) where the function J is explicitly given in terms of $\hat{g}_f$ and $\hat{f}$ by equation (2.18).

3 Reconstruction Algorithm

3.1 PET Algorithm

Taking the real part of equation (1.6) it follows that $f(x_1, x_2)$ is given by

$$f(x_1, x_2) = -\frac{1}{4\pi^2} \int_0^{2\pi} h_\rho(\rho, \theta) \mathrm{d}\theta, \tag{3.1}$$

where $h(\rho, \theta)$ is defined by equation (1.9).

We assume that $f(x_1, x_2)$ has compact support, namely $f(x_1, x_2) = 0$, for ${x_1}^2 + {x_2}^2 \geq 1$. For the numerical calculation of the integral in (3.1) we use the formula

$$\int_0^{2\pi} g(\theta) \mathrm{d}\theta = \frac{2\pi}{N} \sum_{i=0}^{N-1} g\left(\frac{2\pi i}{N}\right). \tag{3.2}$$

Since g is analytic and periodic, this equispaced quadrature converges at spectral speed [36]. In other words, (3.2) represents the optimal quadrature formula for the above integral and its implementation is likely to result in high precision even for relatively small values of N. For the numerical calculation of $h_\rho(\rho, \theta)$ we suppose that $\hat{f}(\rho, \theta)$ is given, for every θ, at n equally spaced points $\rho_i \in [-1, 1]$, i.e. we suppose that $\hat{f}_i = \hat{f}(\rho_i, \theta)$ are known. Moreover, in each interval $[\rho_i, \rho_{i+1}]$ we approximate $\hat{f}(\rho, \theta)$ using the relation

$$\hat{f}(\rho, \theta) = S_i(\rho, \theta) = A_i \hat{f}_i + B_i \hat{f}_{i+1} + C_i \hat{f}_i'' + D_i \hat{f}_{i+1}'', \tag{3.3}$$

where

$$A_i = \frac{\rho_{i+1} - \rho}{\rho_{i+1} - \rho_i}, \quad B_i = 1 - A_i, \quad C_i = \frac{1}{6}({A_i}^3 - A_i)(\rho_{i+1} - \rho_i)^2, \quad D_i = \frac{1}{6}({B_i}^3 - B_i)(\rho_{i+1} - \rho_i)^2,$$

and $\hat{f}_i''$ denotes the second derivative of $\hat{f}(\rho, \theta)$ with respect to ρ, at $\rho = \rho_i$. In other words, we approximate $\hat{f}(\rho, \theta)$ by a cubic spline (in ρ) with equally–spaced nodes. Integrating the spline, we derive a well–known quadrature formula which, in our setting, reads

$$h(\rho, \theta) = \sum_{i=1}^{n-1} \int_{\rho_i}^{\rho_{i+1}} \frac{S_i(\rho', \theta)}{\rho' - \rho} \mathrm{d}\rho'.$$

Following straightforward calculations we obtain

$$\begin{aligned} h_\rho(\rho, \theta) &= \sum_{i=1}^{n-1} \left\{ \frac{\hat{f}_i}{\rho_i - \rho} - \frac{\hat{f}_{i+1}}{\rho_{i+1} - \rho} - \frac{1}{4}(\rho_i - 3\rho_{i+1} + 2\rho)\hat{f}_i'' - \frac{1}{4}(3\rho_i - \rho_{i+1} - 2\rho)\hat{f}_{i+1}'' \right. \\ &+ \left[\frac{\hat{f}_i - \hat{f}_{i+1}}{\rho_i - \rho_{i+1}} - \frac{1}{6}\left(\rho_i - \rho_{i+1} - \frac{3(\rho_{i+1} - \rho)^2}{\rho_i - \rho_{i+1}}\right)\hat{f}_i'' \right. \\ &+ \left. \left. \frac{1}{6}\left(\rho_i - \rho_{i+1} - \frac{3(\rho_i - \rho)^2}{\rho_i - \rho_{i+1}}\right)\hat{f}_{i+1}'' \right] \ln\left|\frac{\rho_{i+1} - \rho}{\rho_i - \rho}\right| \right\}. \end{aligned} \tag{3.4}$$

In order to calculate numerically $f(x_1, x_2)$ from the data $\hat{f}(\rho, \theta)$ we first compute the second derivatives $\hat{f}_i''$. For this purpose we used the subroutine `spline` from Numerical

Recipes [37], setting $\hat{f}_1'' = \hat{f}_n'' = 0$ (i.e. we use the natural cubic spline interpolation). Then, for any x_1 and x_2, we calculate (for any θ) ρ using (2.10b) and $h_\rho(\rho,\theta)$ using (3.4). Finally we calculate $f(x_1,x_2)$ using (3.1).

We note that (3.4) contains the term

$$\ln\left|\frac{\rho_{i+1}-\rho}{\rho_i-\rho}\right|.$$

However, since for the reconstruction the number of the points for x_1 and x_2 can be different than the number of the ρ points, in general $\rho \neq \rho_{i+1}$ and $\rho \neq \rho_i$.

3.2 SPECT Algorithm

We denote the first exponential term of the right–hand side of (2.18) by $I(\tau,\rho,\theta)$, i.e.

$$I(\tau,\rho,\theta) = \exp\left[\int_\tau^{\sqrt{1-\rho^2}} F(\tau',\rho,\theta)\mathrm{d}\tau'\right]. \tag{3.5}$$

Note that, since we have assumed compact support, the integration domain is finite, i.e. $[\tau, \sqrt{1-\rho^2}]$, and $F(\tau,\rho,\theta) = 0$ for $|\rho| \geq 1$, or for $|\tau| \geq \sqrt{1-\rho^2}$.

The definitions (2.4) become

$$P^\pm \hat{f}(\rho,\theta) = \pm\frac{1}{2}\hat{f}(\rho,\theta) - \frac{\mathrm{i}}{2\pi}h(\rho,\theta).$$

Moreover

$$\exp\left[P^\pm \hat{f}(\rho,\theta)\right] = \exp\left[\pm\frac{1}{2}\hat{f}(\rho,\theta)\right]\left(\cos\frac{h(\rho,\theta)}{2\pi} - \mathrm{i}\sin\frac{h(\rho,\theta)}{2\pi}\right),$$
$$\exp\left[-P^\pm \hat{f}(\rho,\theta)\right] = \exp\left[\mp\frac{1}{2}\hat{f}(\rho,\theta)\right]\left(\cos\frac{h(\rho,\theta)}{2\pi} + \mathrm{i}\sin\frac{h(\rho,\theta)}{2\pi}\right).$$

We introduce the following notation:

$$f^{cpe}(\rho,\theta) = \mathrm{e}^{\frac{1}{2}\hat{f}(\rho,\theta)}\cos\frac{h(\rho,\theta)}{2\pi}, \quad f^{spe}(\rho,\theta) = \mathrm{e}^{\frac{1}{2}\hat{f}(\rho,\theta)}\sin\frac{h(\rho,\theta)}{2\pi}, \tag{3.6}$$
$$f^{cme}(\rho,\theta) = \mathrm{e}^{-\frac{1}{2}\hat{f}(\rho,\theta)}\cos\frac{h(\rho,\theta)}{2\pi}, \quad f^{sme}(\rho,\theta) = \mathrm{e}^{-\frac{1}{2}\hat{f}(\rho,\theta)}\sin\frac{h(\rho,\theta)}{2\pi}, \tag{3.7}$$
$$f^{c}(\rho,\theta) = f^{cpe}(\rho,\theta)\hat{g}_f(\rho,\theta), \quad f^{s}(\rho,\theta) = f^{spe}(\rho,\theta)\hat{g}_f(\rho,\theta). \tag{3.8}$$

Using this notation and setting $R(\tau,\rho,\theta) = -J(\tau,\rho,\theta)$, after some calculations, equation (2.18) becomes

$$R(\tau,\rho,\theta) = I(\tau,\rho,\theta)\left((f^{cme} - \mathrm{i}f^{sme})(P^- f^c + \mathrm{i}P^- f^s) + (f^{cme} + \mathrm{i}f^{sme})(P^+ f^c - \mathrm{i}P^+ f^s)\right). \tag{3.9}$$

We now set

$$⨍_{-\infty}^{\infty} \frac{f^c(\rho',\theta)}{\rho'-\rho}\mathrm{d}\rho' = h^c(\rho,\theta), \quad ⨍_{-\infty}^{\infty} \frac{f^s(\rho',\theta)}{\rho'-\rho}\mathrm{d}\rho' = h^s(\rho,\theta),$$

thus equation (3.9) becomes

$$R(\tau,\rho,\theta) = -\mathrm{i}I(\tau,\rho,\theta)\left(f^{cme}\left(\frac{1}{\pi}h^c + 2f^s\right) + f^{sme}\left(\frac{1}{\pi}h^s - 2f^c\right)\right).$$

We denote the right–hand side of this equation by $-\mathrm{i}r(\tau,\rho,\theta)$. Taking the real part of $g(x_1,x_2)$ in (2.19), we obtain

$$g(x_1,x_2) = \frac{1}{4\pi}\int_0^{2\pi}(r_{x_1}\sin\theta - r_{x_2}\cos\theta)\,\mathrm{d}\theta, \tag{3.10}$$

where τ and ρ are given by (2.10) and

$$r(\tau,\rho,\theta) = I(\tau,\rho,\theta)\left(f^{cme}\left(\frac{1}{\pi}h^c + 2f^s\right) + f^{sme}\left(\frac{1}{\pi}h^s - 2f^c\right)\right). \tag{3.11}$$

For the numerical calculation of the Hilbert transform we write

$$\begin{aligned} h(\rho,\theta) &= \int_{-1}^{1}\frac{\hat{f}(\rho,\theta)}{\rho'-\rho}\mathrm{d}\rho' + \int_{-1}^{1}\frac{\hat{f}(\rho',\theta)-\hat{f}(\rho,\theta)}{\rho'-\rho}\mathrm{d}\rho' \\ &= \hat{f}(\rho,\theta)\ln\left(\frac{1-\rho}{1+\rho}\right) + \sum_{i=1}^{n-1}\int_{\rho_i}^{\rho_{i+1}}\frac{S_i(\rho',\theta)-\hat{f}(\rho,\theta)}{\rho'-\rho}\mathrm{d}\rho'. \end{aligned} \tag{3.12}$$

If $\rho=\rho_i$ or $\rho=\rho_{i+1}$ the integral in the right–hand side of (3.12) can be written

$$\int_{\rho_i}^{\rho_{i+1}}\frac{S_i(\rho',\theta)-S_i(\rho,\theta)}{\rho'-\rho}\mathrm{d}\rho'.$$

Thus, after some calculations, we obtain

$$\begin{aligned} &\int_{\rho_i}^{\rho_{i+1}}\frac{S_i(\rho',\theta)-\hat{f}(\rho,\theta)}{\rho'-\rho}\mathrm{d}\rho' = -\hat{f}_i + \hat{f}_{i+1} \\ &+\frac{1}{36}\left(4{\rho_i}^2 - 5\rho_i\rho_{i+1} - 5{\rho_{i+1}}^2 - 3(\rho_i - 5\rho_{i+1})\rho - 6\rho^2\right)\hat{f}_i'' \\ &+\frac{1}{36}\left(5{\rho_i}^2 + 5\rho_i\rho_{i+1} - 4{\rho_{i+1}}^2 - 3(5\rho_i - \rho_{i+1})\rho + 6\rho^2\right)\hat{f}_{i+1}''. \end{aligned} \tag{3.13}$$

If now $\rho\neq\rho_i$ and $\rho\neq\rho_{i+1}$ the integral in the right–hand side of (3.12) can be written

$$\int_{\rho_i}^{\rho_{i+1}}\frac{S_i(\rho',\theta)}{\rho'-\rho}\mathrm{d}\rho' - \hat{f}(\rho,\theta)\ln\left|\frac{\rho_{i+1}-\rho}{\rho_i-\rho}\right|,$$

and after some calculation we obtain

$$\begin{aligned} h(\rho,\theta) &= \sum_{i=1}^{n-1}\left\{F_i - \frac{1}{\rho_i-\rho_{i+1}}\ln\left|\frac{\rho_{i+1}-\rho}{\rho_i-\rho}\right|\left[(\rho_{i+1}-\rho)\hat{f}_i - (\rho_i-\rho)\hat{f}_{i+1}\right.\right. \\ &- \left.\left.\frac{1}{6}(\rho_i-\rho)(\rho_{i+1}-\rho)\left((\rho_i - 2\rho_{i+1} + \rho)\hat{f}_i'' + (2\rho_i - \rho_{i+1} - \rho)\hat{f}_{i+1}''\right)\right]\right\} \end{aligned} \tag{3.14}$$

where F_i is the right–hand side of (3.13).

In order to calculate numerically $I(\tau,\rho,\theta)$ for any x_1, x_2 and θ we use relations (3.1) and (2.10b). Thus

$$f(x_1,x_2)=-\frac{1}{4\pi^2}\int_0^{2\pi}h_\rho(x_2\cos t-x_1\sin t,t)\mathrm{d}t$$

and consequently

$$F(\tau,\rho,\theta)=-\frac{1}{4\pi^2}\int_0^{2\pi}h_\rho(\tau\sin(\theta-t)+\rho\cos(\theta-t),t)\mathrm{d}t, \tag{3.15}$$

where τ and ρ are given from (2.10) and h_ρ from (3.4). We can now calculate $F(\tau,\rho,\theta)$ following the procedure outlined in the previous section. We then calculate $I(\tau,\rho,\theta)$ using relation (3.5) if $\tau\geq 0$, alternatively the relation

$$I(\tau,\rho,\theta)=\exp\left[\hat{f}(\rho,\theta)-\int_{-\sqrt{1-\rho^2}}^{\tau}F(\tau',\rho,\theta)\mathrm{d}\tau'\right] \tag{3.16}$$

if $\tau<0$. For the numerical calculation of the integrals appearing in (3.5) and (3.16) we use the Gauss–Legendre quadrature with two functional evaluations at every step, i.e.

$$\int_\alpha^\beta F(\tau',\rho,\theta)\mathrm{d}\tau'\approx w_1F(\tau_1,\rho,\theta)+w_2F(\tau_2,\rho,\theta),$$

where the abscissas τ_1, τ_2 and the weights w_1, w_2 are given by

$$\tau_1=\alpha+(\beta-\alpha)\left(\frac{1}{2}-\frac{\sqrt{3}}{6}\right),\quad \tau_2=\alpha+(\beta-\alpha)\left(\frac{1}{2}+\frac{\sqrt{3}}{6}\right),\quad w_1=w_2=\frac{1}{2}(\beta-\alpha).$$

We also notice that we have tried subdivision of the interval (α,β) into several intervals and the improvement is very minor. Therefore we use just one interval, i.e. two function evaluations per quadrature, since the major increase in running time of the program implicit in using panel quadrature is not justified by the modest improvement in accuracy.

For the numerical calculation of the integrals in (3.10) and (3.15) we use again formula (3.2), resulting in spectral convergence. For the numerical calculation of the partial derivatives r_{x_1} and r_{x_2} in (3.10) we use the forward difference scheme

$$f'(x)\approx\frac{-3f(x)+4f(x+\Delta x)-f(x+2\Delta x)}{2\Delta x}$$

for the first half of the interval $[-1,1]$, and the backward difference scheme

$$f'(x)\approx\frac{3f(x)-4f(x-\Delta x)+f(x-2\Delta x)}{2\Delta x}$$

for the second half.

Thus, for the numerical calculation of $g(x_1,x_2)$ from the data $\hat{f}(\rho,\theta)$ and $\hat{g}_f(\rho,\theta)$ we apply the following procedure: First we calculate the second derivatives $\hat{f}_i''$, using subroutine `spline`. Consequently, we calculate $h(\rho,\theta)$ using (3.12) and (3.13) for all given ρ and θ. Notice that if $|\rho_i|=1$, then, since we have assumed compact support,

$\hat{f}(\rho,\theta) = 0$, thus the first term in (3.12) is absent. We then calculate $f^{cpe}(\rho,\theta)$ and $f^{spe}(\rho,\theta)$ using (3.6), as well as $f^{c}(\rho,\theta)$ and $f^{s}(\rho,\theta)$ using (3.8) (at this stage we use the second data function $\hat{g}_f$). Finally we calculate, again using `spline`, the second derivatives for the natural cubic spline interpolation of the functions $f^{c}(\rho,\theta)$ and $f^{s}(\rho,\theta)$.

Having calculated all the necessary second derivatives we now proceed as follows: First we calculate $\hat{f}(\rho,\theta)$ for any x_1, x_2 (and θ) using (2.10) and (3.3). For this purpose we have used subroutine `splint` from Numerical Recipes. Consequently we calculate $h(\rho,\theta)$ using (3.14). Then we calculate $f^{cme}(\rho,\theta)$ and $f^{sme}(\rho,\theta)$ using (3.7), $f^{c}(\rho,\theta)$ and $f^{s}(\rho,\theta)$ using `splint` and finally $h^{c}(\rho,\theta)$ and $h^{s}(\rho,\theta)$ using relations similar to (3.14). These last six functions are used in (3.11). We then calculate $I(\tau,\rho,\theta)$ as described earlier. Finally we calculate $r(\tau,\rho,\theta)$ using (3.11) and consequently $g(x_1,x_2)$ using (3.10).

4 Numerical Tests

The θ points are equally spaced in $[0,2\pi]$, while the ρ points are equally spaced in $[-1,1]$. The density plots presented below were drawn by using `Mathematica` [38]. The dark color represents zero (or negative) values while the white color represents the maximum value of the original (or reconstructed) function.

First we tested the PET algorithm for the three different phantoms shown in Figures 3. Figures (a) and (b) were taken from [28] and [30], respectively. These figures depict the attenuation coefficient for a function $f(x_1,x_2)$ modelling a section of a human thorax. The small circles represent bones and the larger ellipses the lungs. Figure (c) is the well known Shepp–Logan phantom, which provides a model of a head section. All these phantoms consist of different ellipses with various densities.

Using the Radon transform (1.4), we computed the data function $\hat{f}(\rho,\theta)$ for 200 points for θ and 100 points for ρ. This computation was carried out by using `Mathematica`. We then used these data in the numerical algorithm to reevaluate $f(x_1,x_2)$. Furthermore, in order to remove the effect of the Gibbs–Wilbraham phenomenon, we applied an averaging filter as follows: We first found the maximum value (max) of $f(x_1,x_2)$ in the reconstructed image. We then set to zero those values of $f(x_1,x_2)$ which were less than $\frac{1}{20}$ max. Finally we applied the averaging filter with averaging parameter $a = 0.005$. This filtering procedure was applied five times, with the additional elimination of those values of $f(x_1,x_2)$ which were less than $\frac{1}{20}$ max at the end of the procedure. In Figures 4 and 5 we present the results before and after the filtering procedure, respectively. The reconstruction took place in a 500×500 grid.

We then tested the SPECT algorithm for the three different phantoms shown in Figures 6. Figures (a) and (b) were taken from [28]. In these cases the function $f(x_1,x_2)$ is given by Figure 3(a). Figure (c) was taken from [30]. The white ring represents the distribution of the radiopharmaceutical at the myocardium. In this case the function $f(x_1,x_2)$ is given by Figure 3(b).

By using the Radon transform (1.4), and the attenuated Radon transform (1.5), we computed the data functions $\hat{f}(\rho,\theta)$ and $\hat{g}_f(\rho,\theta)$ for 200 values of θ and 100 points of ρ (again using `Mathematica`). We consequently used these data in our program to re–evaluate $g(x_1,x_2)$. In order to remove the effect of the Gibbs–Wilbraham phenomenon, a median filter was used, with the additional elimination of those values of $g(x_1,x_2)$ which were less than $\frac{1}{20}$ max before and after the application of the filter. The results

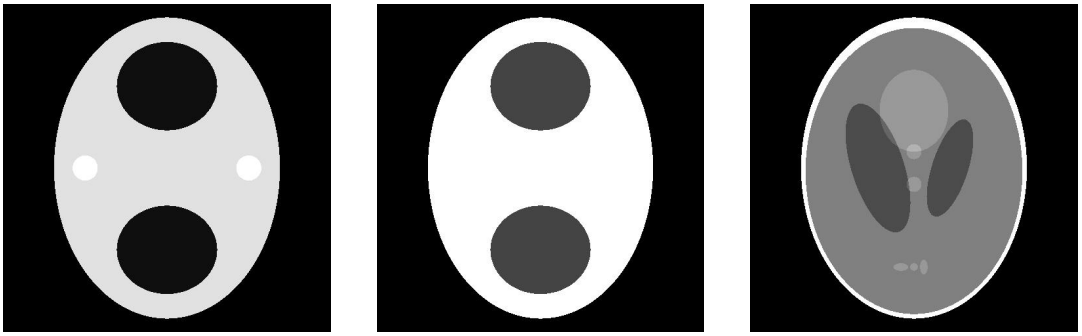

(a) (b) (c)

Figure 3: Test phantoms for the PET algorithm.

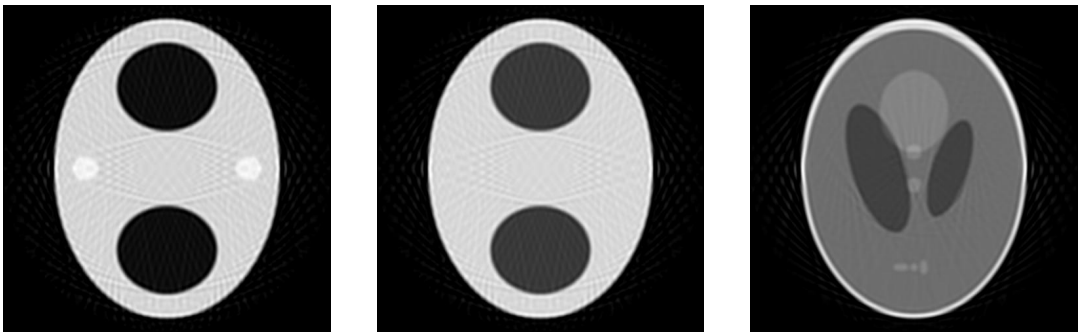

(a) (b) (c)

Figure 4: The reconstruction of the phantoms of Figures 3 before the filtering procedure.

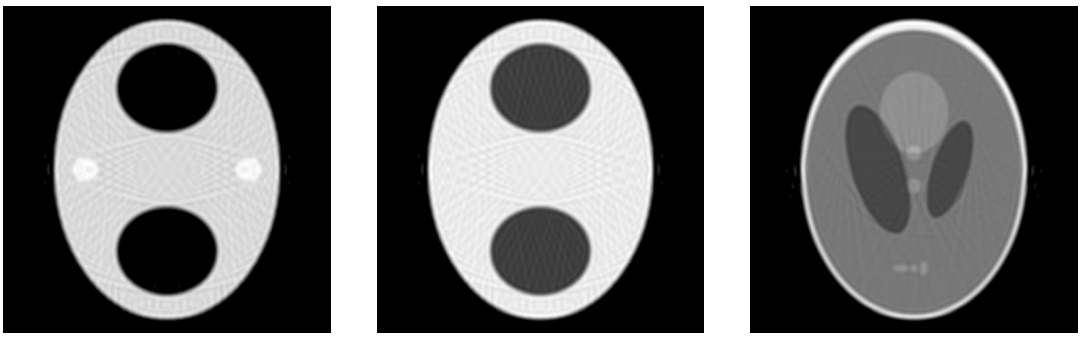

(a) (b) (c)

Figure 5: The reconstruction of the phantoms of Figures 3 after the filtering procedure.

are shown in Figures 7 and 8, before and after the filtering procedure respectively. The reconstruction took place in a 140×140 grid.

For the above phantoms it seems that even a rough estimation of $F(\tau, \rho, \theta)$ is sufficient for an accurate reconstruction. This means that, in order to compute numerically $F(\tau, \rho, \theta)$ using (3.15), it is sufficient to use ten equally spaced points for t, rather than 200. This reduces considerably the reconstruction time.

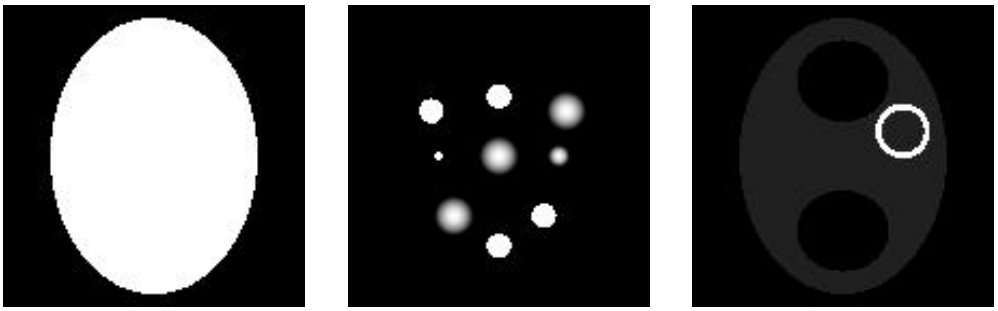

(a) (b) (c)

Figure 6: Test phantoms for the SPECT algorithm. In Figures (a) and (b) the function $f(x_1, x_2)$ is given by Figure 3(a), while in Figure (c) the function $f(x_1, x_2)$ is given by Figure 3(b).

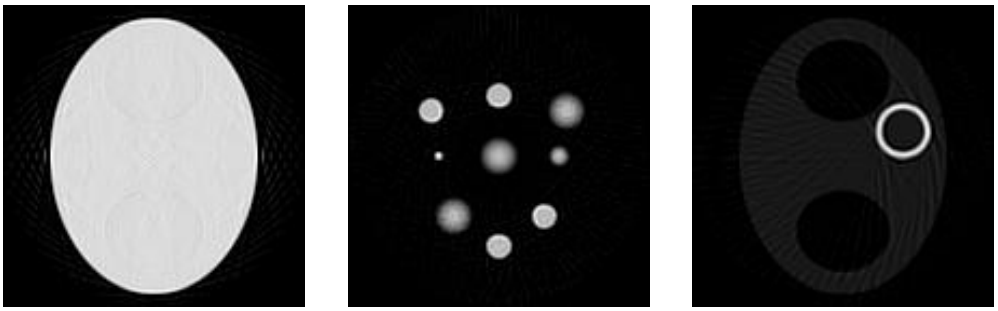

(a) (b) (c)

Figure 7: The reconstruction of the phantoms of Figures 6 before the filtering procedure.

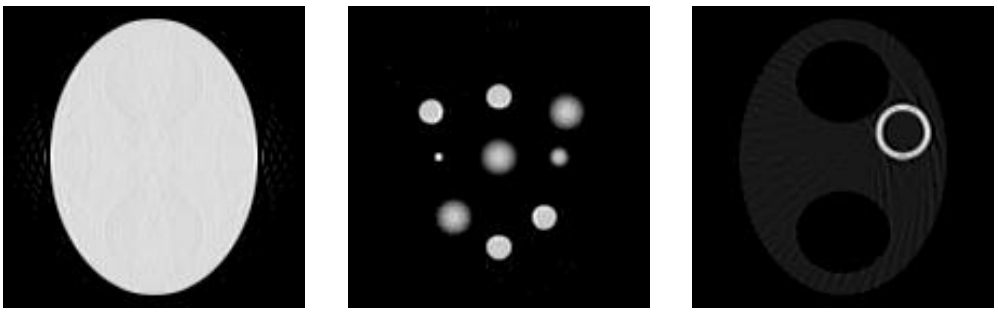

(a) (b) (c)

Figure 8: The reconstruction of the phantoms of Figures 6 after the filtering procedure.

Acknowledgments

V.M. was supported by a Marie Curie Individual Fellowship of the European Community under contract number HPMF-CT-2002-01597. We are grateful to Professor B. Hutton for useful suggestions.

References

[1] D. Koh, G.J.R. Cook, J.E. Husband, New Horizons in Oncologic Imaging (editorial), N. Engl. J. Med. **348**, 2487 (2003).

[2] J. Jonides et al., Verbal and Spatial Working Memory in Humans, Psychol. Learn. Motiv. **35**, 43 (1996).

[3] G.S. Mark et al., Understanding Emotional Prosody Activates Right Hemisphere Regions, Arch. Neurol. **53**, 665 (1996).

[4] S. Vorstrup, O.B. Paulson, N.A. Lassen, Cerebral Blood Flow in Acute and Chronic Ischemic Stroke using Xenon–133 Inhalation Tomography, Acta Neurol. Scand. **74**, 439 (1986).

[5] M. Lauritzen, J. Olesen, Regional Cerebral Blood Flow During Migraine Attacks by Xenon–133 Inhalation and Emission Tomography, Brain **107**, 447 (1984).

[6] B.I. Lee et al., HIPDM–SPECT in Patients with Medically Intractable Complex Partial Seizures: Ictal study, Arch. Neurol. **45**, 397 (1988).

[7] J.L. Tyler, T.N. Byme, Neoplastic Disorders, in *Clinical Brain Imaging: Principles and Applications*, eds. J.C. Mazziotta, S. Gilman, p 166, Philadelphia: F.A. Davis (1992).

[8] J.C. Mazziotta, Movement Disorders, in *Clinical Brain Imaging: Principles and Applications*, eds. J.C. Mazziotta, S. Gilman, p 244, Philadelphia: F.A. Davis (1992).

[9] S. Minoshima et al., A Diagnostic Approach in Alzheimer's Disease Using Three–Dimensional Stereotactic Surface Projections of Fluorine–18–FDG PET, J. Nucl. Med. **36**, 1238 (1995).

[10] L. Junck et al., PET Imaging of Human Gliomas with Ligands for the Peripheral Benzodiazepine Binding Site, Ann. Neurol. **26**, 752 (1989).

[11] J.C. Mazziotta et al., Reduced Cerebral Glucose Metabolism in Asymptomatic Subjects at Risk for Huntington's Disease, N. Engl. J. Med. **316**, 357 (1987).

[12] N.C. Andreasen, Linking Mind and Brain in the Study of Mental Illnesses: A Project for a Scientific Psychopathology, Sci. **275**, 1586 (1997).

[13] E.M. Reiman et al., Neuroanatomical Correlates of Anticipatory Anxiety, Sci. **243**, 1071 (1989).

[14] J.G. Tjuvajev et al., A General Approach to the Non–Invasive Imaging of Transgenes using Cis–Linked Herpes Simplex Virus Thymidine Kinase, Neoplasia **1**, 315 (1999).

[15] Y. Yu et al., Quantification of Target Gene Expression by Imaging Reporter Gene Expression in Living Animals, Nature Med. **6**, 933 (2000).

[16] L.A. Green et al., Indirect Monitoring of Endogenous Gene Expression by Positron Emission Tomography (PET) Imaging of Reporter Gene Expression in Transgenic Mice, Mol. Imaging Biol. **4**, 71 (2002).

[17] M. Doubrovin et al., Imaging Transcriptional Regulation of p53–Dependent Genes with Positron Emission Tomography in Vivo, Proc. Natl Acad. Sci. USA, **98**, 9300 (2001).

[18] D. Lardinois et al., Staging of Non–Small–Cell Lung Cancer with Integrated Positron–Emission Tomography and Computed Tomography, N. Engl. J. Med. **348**, 2500 (2003).

[19] D. Ost, A.M. Fein, S.H. Feinsilver, The Solitary Pulmonary Nodule, N. Engl. J. Med. **348**, 2535 (2003).

[20] B.F. Hutton, Cardiac Single–Photon Emission Tomography: Is Attenuation Correction Enough? (invited editorial), Eur. J. Nucl. Med. **24**, 713 (1997).

[21] F.J.T. Wackers, Attenuation Correction, or the Emperor's new Clothes? (editorial), J. Nucl. Med. **40**, 1310 (1999).

[22] F.M. Bengel et al., Effect of Sympathetic Reinnervation on Cardiac Performance after Heart Transplantation, N. Engl. J. Med. **345**, 731 (2001).

[23] F. Natterer, *The Mathematics of Computerized Tomography*, Wiley, New York (1986).

[24] A.S. Fokas, R.G. Novikov, Discrete Analogues of $\overline{\partial}$–Equations and of Radon Transform, C. R. Acad. Sci. Paris Ser. I. Math. **313**, 75 (1991).

[25] R.G. Novikov, An Inversion Formula for the Attenuated X–ray Transformation, Ark. Mat. **40**, 145 (2002).

[26] L.A. Shepp, B.F. Logan, The Fourier Reconstruction of a Head Section, IEEE Trans. Nucl. Sci. **21**, 21 (1974).

[27] F. Natterer, Inversion of the Attenuated Radon Transform, Inv. Prob. **17**, 113 (2001).

[28] L.A. Kunyansky, A New SPECT Reconstruction Algorithm Based on the Novikov Explicit Inversion Formula, Inv. Prob. **17**, 293 (2001).

[29] J.P. Guillement, F. Jauberteau, L. Kunyansky, R. Novikov, R. Trebossen, On Single Photon Emission Computed Tomography Imaging based on an Exact Formula for the Nonuniform Attenuation Correction, Inv. Prob. **18**, L11 (2002).

[30] J.P. Guillement, R.G. Novikov, A Noise Property Analysis of Single–Photon Emission Computed Tomography Data, Inv. Prob. **20**, 175 (2004).

[31] T. Hebert, R. Leahy, M. Singh, Fast MLE for SPECT using an Intermediate Polar Representation and a Stopping Criterion, IEEE Trans. Nucl. Sci. **35**, 615 (1988).

[32] Z. Liang, H. Hart, Bayesian Reconstruction in Emission Computed Tomography, IEEE Trans. Nucl. Sci. **35**, 788 (1988).

[33] J. Nuyts, J.A. Fessler, A Penalized–Likelihood Image Reconstruction Method for Emission Tomography, compared to Post–Smoothed Maximum–Likelihood with Mached Spatial Resolution, IEEE Trans. Med. Imag. **22**, 1042 (2003).

[34] A.S. Fokas, I.M. Gel'fand, Integrability of Linear and Nonlinear Evolution Equations, and the Associated Nonlinear Fourier Transforms, Lett. Math. Phys. **32**, 189 (1994).

[35] M.J. Ablowitz, A.S. Fokas, *Introduction and Applications of Complex Variables*, Cambridge University Press (1997).

[36] B. Fornberg, A Practical Guide to Pseudospectral Methods, Cambridge University Press (1996).

[37] W.H. Press, S.A. Teukolsky, W.T. Vetterling, B.P. Flannery, *Numerical Recipes in Fortran. The Art of Scientific Computing (2nd edition)*, Cambridge University Press (1992).

[38] S. Wolfram, *The Mathematica Book (4th edition)*, Cambridge University Press (1999).